



**HAL**  
open science

## Coupling and robustness of intra-cortical vascular territories

Romain Guibert, Caroline Fonta, Laurent Risser, Franck Plouraboué

► **To cite this version:**

Romain Guibert, Caroline Fonta, Laurent Risser, Franck Plouraboué. Coupling and robustness of intra-cortical vascular territories. *NeuroImage*, 2012, vol. 62 (1), pp.408-417. 10.1016/j.neuroimage.2012.04.030 . hal-00714836

**HAL Id: hal-00714836**

**<https://hal.science/hal-00714836>**

Submitted on 5 Jul 2012

**HAL** is a multi-disciplinary open access archive for the deposit and dissemination of scientific research documents, whether they are published or not. The documents may come from teaching and research institutions in France or abroad, or from public or private research centers.

L'archive ouverte pluridisciplinaire **HAL**, est destinée au dépôt et à la diffusion de documents scientifiques de niveau recherche, publiés ou non, émanant des établissements d'enseignement et de recherche français ou étrangers, des laboratoires publics ou privés.



## Open Archive Toulouse Archive Ouverte (OATAO)

OATAO is an open access repository that collects the work of Toulouse researchers and makes it freely available over the web where possible.

This is an author-deposited version published in: <http://oatao.univ-toulouse.fr/>  
Eprints ID: 6021

**To link to this article:**

<http://dx.doi.org/10.1016/j.neuroimage.2012.04.030>

**To cite this version** : Guibert, Romain and Fonta, Caroline and Risser, Laurent and Plouraboué, Franck *Coupling and robustness of intra-cortical vascular territories*. (2012) NeuroImage, vol. 62 (n° 1). pp. 408-417. ISSN 1053-8119

Any correspondence concerning this service should be sent to the repository administrator: [staff-oatao@inp-toulouse.fr](mailto:staff-oatao@inp-toulouse.fr)

# Coupling and robustness of intra-cortical vascular territories

Romain Guibert <sup>a,b,1</sup>, Caroline Fonta <sup>b</sup>, Laurent Risser <sup>c</sup>, Franck Plouraboué <sup>a,\*</sup>

<sup>a</sup> Institut de Mécanique des Fluides, UMR 5502, INPT-CNRS-UPS, 1 Allée du Professeur Camille Soula, 31400 Toulouse, France

<sup>b</sup> Centre de recherche Cerveau et Cognition, UMR 5549, CNRS-UPS, Pavillon Baudot, CHU Purpan, BP 25202, 31052 Toulouse Cedex 3, France

<sup>c</sup> Institute of Biomedical Engineering, University of Oxford, Oxford OX3 7DQ, UK

## A B S T R A C T

Vascular domains have been described as being coupled to neuronal functional units enabling dynamic blood supply to the cerebral cyto-architecture. Recent experiments have shown that penetrating arterioles of the grey matter are the building blocks for such units. Nevertheless, vascular territories are still poorly known, as the collection and analysis of large three-dimensional micro-vascular networks are difficult. By using an exhaustive reconstruction of the micro-vascular network in an 18 mm<sup>3</sup> volume of marmoset cerebral cortex, we numerically computed the blood flow in each blood vessel. We thus defined arterial and venular territories and examined their overlap. A large part of the intracortical vascular network was found to be supplied by several arteries and drained by several venules. We quantified this multiple potential to compensate for deficiencies by introducing a new robustness parameter. Robustness proved to be positively correlated with cortical depth and a systematic investigation of coupling maps indicated local patterns of overlap between neighbouring arteries and neighbouring venules. However, arterio-venular coupling did not have a spatial pattern of overlap but showed locally preferential functional coupling, especially of one artery with two venules, supporting the notion of vascular units. We concluded that intra-cortical perfusion in the primate was characterised by both very narrow functional beds and a large capacity for compensatory redistribution, far beyond the nearest neighbour collaterals.

## Keywords:

Brain blood flow  
Haemodynamics  
Vascular territories  
Venule-arteriole coupling  
Collateral supply

## Introduction

Micro-vascular networks are complex and their organisational structure is organ-specific. Cortical vessel networks are highly interconnected, with blood flow in them continuously controlled because brain activity never ceases and oxygen and nutrients cannot be stored in cortical tissues. The cortical vascular system is structured by the highly reticulated pial surface vascular network, which plunges down into a set of penetrating vessels. It is tempting to attribute a vascular domain to each penetrating arteriole. Recent high-resolution MRI scanners allow the non-invasive acquisition of intra-cortical vessels, permitting arteries and venules to be discriminated (Harel et al., 2010). Their increasing resolution holds promise of enabling BOLD fMRI sequences to be associated with the underlying vascular system. This opens up the possibilities of probing the cortical organisation into columnar, modular and laminar domains and testing the coupling between neuronal functional assemblies and

vascular domains. This coupling has been observed for the barrel cortex by using invasive techniques in animal models (Woolsey et al., 1996) and has been suggested by anatomical studies in the primate visual cortex (Bell and Ball, 1985; Fonta and Imbert, 2002; Zheng et al., 1991), although its control mechanisms have not been clearly established (Rossier, 2009). Interestingly, Harel and co-workers' studies (Harel et al., 2010) on the visual cortex, which is highly organised into modules (ocular dominance columns, orientation columns, blobs, etc.), showed that BOLD variations following visual stimulations were non-uniform across the visual cortex and through the cortical depth. The largest ones also involved large intracortical veins. Based on their own observations and on the qualitative anatomical description by Duvernoy et al. (1981), Harel and co-workers (2010) put forward the hypothesis of vascular units. Such units would rely on the arrangement of arteries around veins in association with groups of neurones involved in a given computational task.

Another strategy for investigating the functional organisation of the cortical micro-vascularisation is to disturb the blood supply and measure the extent of the perturbation induced in the blood flow. Very elegant experiments designed to disrupt blood flow in a single arteriole in rodents (Schaffer et al., 2006; Sigler et al., 2008) have measured the impact of occluding a single penetrating artery in a cortical domain around the clotted artery (Nishimura et al., 2006). The authors thus defined an arteriole territory of about 500 µm in diameter, associated with damaged cerebral tissue (Nishimura et al.,

\* Corresponding author at: Institut de Mécanique des Fluides de Toulouse, 1 Allée du Professeur Camille Soula, 31400 Toulouse, France. Fax: +33 5 34 32 78 99.

E-mail addresses: romainguibert@gmail.com (R. Guibert), caroline.fonta@cerco.ups-tlse.fr (C. Fonta), laurent.risser@gmail.com (L. Risser), franck.plouraboue@imft.fr (F. Plouraboué).

<sup>1</sup> Present address: REO project—INRIA Rocquencourt, BP 105-78153 Le Chesnay Cedex, France.

2007). These observations are valid only for the upper part of the cortex since scattering and absorption limit the penetration of light into tissues *in vivo*, thus imposing limitations on two-photon imaging techniques. Moreover, they show that the blood flow perturbations are not compensated by active changes in the diameter of neighbouring arteries, suggesting a lack of signalling to recruit compensatory vaso-regulatory mechanisms (Nishimura et al., 2010). Thus, at this level of the intra-cortical vascular network, compensatory mechanisms would be passive and result from a coupling between vessels. Collateral circulation is an important aspect of cerebrovascular flow which remains largely unappreciated (Liebeskind, 2003). At the micro-vascular scale, its lack of assessment partly results from the limits of experimental approaches. Experimental studies face restrictions on the volume of the cortex samples that can be analysed. Also, they cannot separate two key factors that control tissue perfusion: the structural properties of the vessel network and the delicate molecular and cellular interplay between the neuronal cells and contractile elements of the vessel walls. Numerical simulations allow an isolated part of the vascular system to be considered and can offer the possibility of characterising a reference condition. In contrast, in experimental conditions, it is difficult to master all physiological parameters related to the internal status of the animal or tissue of interest, which, through intravascular or parenchymal components, can exert local or widespread control of blood flow (Itoh and Suzuki, 2012). For *in-vivo* experiments, for example, the impact of subcortical pathways, which pilot the intra-cortical neuro-vascular units, cannot be isolated (Hamel, 2006). There is therefore a need for basic knowledge about the anatomic-functional organisation of the micro-vascular network. Vessel networks are highly connected structures, whose design (vessel diameter, curvature, topology) contributes largely to the haemodynamic characteristics of blood flow (Guibert et al., 2010a). Thus a spatial description alone of the vascular network cannot account for the perfusion modalities. Many detailed aspects are poorly known, in the absence of any external stimulation or internal uncontrolled physiological input: the vascular domain perfused by an artery, the structural and functional coupling, i.e. blood flow perfusion, between arteriolar, between venular, or between arteriolar and venular domains, as well as their possible overlap. This information is an essential element in the interpretation of BOLD fMRI brain investigations or neuro-vascular coupling analyses, and would promote understanding of the collateral perfusion which might be relevant in various pathological situations.

The goal of our contribution is to fill this gap and to provide clear identification and quantification of “network induced” perfusion, i.e. passive perfusion in absence of diameter variations, and compensatory capacity. For this, we used haemodynamic simulation inside realistically large volumes of vascular networks of the primate cortex. *In-silico* simulations can go beyond the limits of experimental analyses and allow systematic investigation of the spatial distribution of the brain perfusion inside a large cortical volume in passive conditions. Beyond this issue, this approach offers the possibility to simulate physiological or pathological conditions that modify the passive vascular network and to evaluate their effects on the microcirculation.

## Material and methods

### *Vessel network imaging and blood flow simulation*

This contribution was based upon animal preparation associated with intra-cardiac injection of highly-concentrated X-ray contrast agent (barium sulphate), from which, after tissue fixation and sample extraction, a synchrotron computed tomography image (Plouraboué et al., 2004) was acquired. After acquisition, image segmentation, vessel skeletonisation, vectorisation and post-processing were performed as described by Risser et al. (2009) and Risser et al. (2007, 2008). Post-processing procedures included image analysis methods,

such as cleaning holes using mathematical morphology open/closure operators and a gap filling method (Risser et al., 2008). After estimation of the vessel centrelines (skeletonisation), each local vessel diameter was estimated by growing a sphere around the centreline as long as the image grey levels were homogeneous within the sphere (Risser et al., 2009). Thus, an 18 mm<sup>3</sup> volume of marmoset monkey cerebral cortex was skeletonised over the whole cortical depth (currently 2 mm). The vascular network extracted was then encoded using a compact, structured representation.

A numerical evaluation of the blood perfusion in this realistic vascular network was then established. We have recently developed a network model which evaluates the flow in each vessel segment at a moderate computational cost. This model takes account of the network geometry, the blood flow rheology, the phase separation and the boundary conditions associated with arterial inputs and venous outputs (Guibert et al., 2010a). The method considers local flux/pressure gradient relationships inside each vessel segment, which generalises Poiseuille’s law for blood flow. In these flow models, the presence of red blood cells increases the local pressure and this is taken care of through an apparent viscosity parameter depending on the local haematocrit, the relative volume of red blood cells in the blood (Fung, 1997; Kiani and Hudetz, 1991; Pries and Secomb, 2005). In this work, we used the model proposed by Pries and Secomb (2005), which takes into account the influence of glycocalyx inside small capillaries. A supplementary hydrodynamic effect called “phase separation” is associated with the haematocrit distribution at bifurcations (Fung, 1997). By integrating the local flow/pressure gradient relationship along the centreline of each vascular segment between two successive bifurcations, we computed the hydraulic conductance of each vascular segment. This conductance gives the local relationship between blood flow in a vascular segment and the pressure drop applied at its upstream and downstream bifurcations. Imposing flow conservation while solving only the pressure values at bifurcations drastically reduces the number of unknown variables to be found. Our previous study has shown that, despite what would be expected from an analysis of small networks only (Guibert et al., 2010b), simulations in realistic networks are not sensitive to the phase separation mechanism as far as the pressure distribution and local flows are concerned. In contrast, we found a strong dependence on the apparent viscosity model. In the network considered in this study, using the apparent viscosity model of Pries and Secomb (2005) with constant haematocrit or with variable haematocrit for different phase separation models, gave very similar results for the predicted blood flows (Guibert et al., 2010a). Therefore, the constant haematocrit condition provided a good approximation for the estimation of the blood flow, which was the main concern of this study since we exclusively considered hydraulic couplings among the various input/outputs. Hence, in the present work, a constant haematocrit condition, equal to 0.45 in the entire network, and a physiological pressure difference of 70 mmHg between arteriolar input and venular output were applied.

It was essential for these studies to correctly identify the vessels perforating the cortical mantle as arterial or venular vessels. Several features were used to reliably distinguish inputs and outputs, as described in Guibert et al. (2010a). The arteriolar pial network showed many anastomoses. Its vessels were brightly textured (image grey levels were almost white inside arterioles), with well defined, smooth borders thanks to the injected contrast agent. Thus, pial arterioles were easy to detect, identify and automatically link to one another. Furthermore, all penetrating arterioles were related to the pial arteriolar network at the cortical surface by a single clear connection. Hence, penetrating arterioles were also easy to distinguish. The venous pial network gave a very different, grainy texture of grey levels with rough boundaries showing occasionally sketchy connections, since the contrast agent distribution in venous vessels was less homogeneous. The venous side was thus easy to distinguish from the

arterial one, so that it was possible to find corresponding venous penetrating vessels. Using these two complementary procedures for the arterial and venous sides removed all ambiguities in the identification of penetrating vessels. Hence, this work identified arterial and venular elements in the pia matter, the fit of penetrating vessels with pial structures, and the heterogeneous quality of vessel penetration by the contrast agent within arteries and venules. Thirty-seven penetrating arterioles and twenty-four draining venules were identified in the cortical sample. This proportion of arteries among penetrating vessels is consistent with previous estimates in primates and humans, i.e. two arteries for three penetrating vessels (Cassot et al., 2009; Weber et al., 2008).

#### Definitions of territories and robustness maps

We investigated different notions for the topological organisation of vascular perfusion. We considered the oriented graph which describes the blood flow into all vascular segments and its direction. From each perforating vessel, we then defined a vascular territory as the entire region spanned for either perfusion (arterial territory, AT), or drainage (venular territory, VT) (Fig. 1). From an algorithmic point of view, AT and VT are very similar concepts, their evaluation only differing by the flux direction. Using this procedure, it is possible for two distinct territories to overlap (Fig. 1A).

Therefore, in order to quantify the redundancy of the perfusion at any point of the vascular network, we specified how many arterioles a given vascular segment could be perfused by. To do so, we defined an index called the robustness index (RI). Its value was set to one at the cortex entry. For each entering penetrating vessel, we evaluated its perfusion territory (i.e. all connected vessels supplied with a non-null flow) inside the network. Using an incremental evaluation of all multiple affiliations of each perfused vessel to any territory, we evaluated the number of entries which could possibly perfuse a given vessel. The RI was incremented by one each time a given vessel was perfused by a given arteriolar entry. Propagating this procedure inside the network and spanning the contribution of all possible entries generated a map of robustness (RM) inside the network (Fig. 1B). For each segment location, the arterial robustness map (ARM) quantified the total number of penetrating arteries contributing to its perfusion. For a given segment, this number is called the arterial robustness index (ARI). Hence, the ARI of a venule gives the total number of input arteries that this venule drains. The complementary concept of venous robustness index (VRI) quantifies, for each vein, the number of VT it collects from. It also represents the number of venules that potentially drain the flow of each arteriole.

An alternative approach for analysing vascular territories aimed to define non-overlapping territories using a selective procedure. This procedure imposed a rule at nodes of convergence between two vascular

segments, the resulting segment being attributed to the territory which supplied the highest flux (Fig. 1C). If we take input flows  $Q_{T1}$  and  $Q_{T2}$  to a given bifurcation which belong to two distinct arterial territories, the attribution rule for the preferential territory  $T_p$  of the vascular segment downstream of the bifurcation can be described by the simple formula

$$\text{if } Q_{T1} = \max(Q_{T1}, Q_{T2}), \text{ then } T_p = T1, \text{ else } T_p = T2 \quad (1)$$

and the same rule applies for veins. This rule can be recursively applied at each bifurcation of the entire network to provide preferential territories (PT) for each input artery (APT) or output venule (VPT).

We could have used more advanced (and possibly more accurate) definitions of specific vascular territories. Nevertheless, a key advantage of the preferential rule defined here lies in its simple and local nature: it is easy to define which artery is the most prominent provider at each bifurcation. The anatomical properties of the different types of territories were quantified and compared in terms of total vessel volume (in cubic millimetres) and length (in millimetres). The vessel length was computed as the curvilinear distance along the skeletonised vessel centrelines (Risser et al., 2009). At a given point of the discretised skeleton, the local diameter and curvilinear length provided a local, longitudinally varying, cylindrical description of the vessel. Summing over the contribution of each locally varying cylindrical shape from the upstream to the downstream bifurcation of a given vessel segment provided its total volume. The total length and volume of a given set of vessel segments were then evaluated as the sum of all vessel segment contributions. The uncertainty on the vessel diameter estimate at specimen preparation has been discussed in Risser et al. (2009), where the authors show that the total volume reduction effect associated with sample dehydration can be dealt with if proper care is taken.

#### Overlapping volume and flow maps

Besides the robustness index, we also analysed territory overlap by evaluating the sum of volumes and flows in all shared vascular segments. After normalising these shared volumes and flows by the total vascular volume and the global cerebral blood flow, we computed the relative overlapping volume and flow between any pair of territories. The global cerebral blood flow was computed by summing the contribution of all penetrating arteriolar input within the considered volume. Given the blood flow conservation principles, this was also the total venous flow, as was consistently verified by computing the sum of output flows from penetrating venules.

Results are illustrated with overlapping maps (Fig. 5), where each input/output vessel lumen location is represented on the cortical surface with a blue (for vein) or red (for artery) sphere. The link thickness

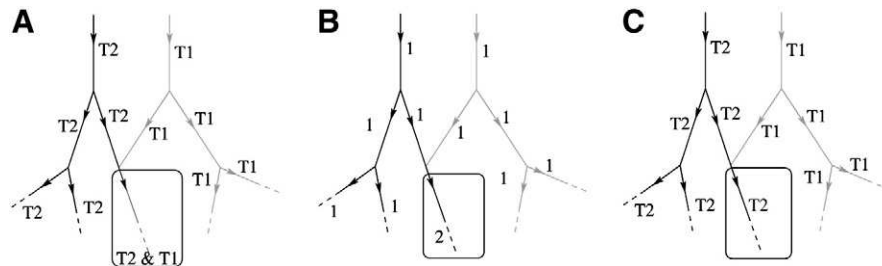


**Fig. 1.** Representation of the notions of territories and robustness. Using blood flow simulation, a vascular territory is defined as the network of segments perfused by a penetrating vessel. In (A) two territories, T1 and T2, are defined. Segments supplied by different inputs, here in the black frame, belong to the overlapping network. From these territories, a robustness map (RM) is computed using the value of the robustness index (RI) attributed to an individual vascular segment. RI value corresponds to the number of inputs which supply each segment (B). For example, for the framed joint segment, supplied by both T1 and T2, RI equals 2, while it is equal to 1 for the other segments irrigated by only one input. The same network can be considered differently by applying a rule at each branching point that imposes that a segment must belong to the territory providing it with the higher flow (for example, in C, the joint segment is attributed to Territory T2). In this case, T1 and T2 are preferential territories without any overlap.

between two spheres is proportional to the value of the overlapping relative volumes or flows of their respective three-dimensional territories.

In the case of preferential territories (PTs), the overlap of any two PTs is null by definition. Nevertheless, PTs are neighbours, by construction. A fraction of any input flow coming from a given PT perfuses through the other PTs, finally leading to the blood being collected in a venous PT. From flow conservation principles, all the input flows entering or leaving a single penetrating vessel are distributed into their neighbour PTs. By computing the sum of all flows going from one PT to another, their absolute preferential territory cross-stream (PTCS) flow can be evaluated. This preferential territory cross-stream flow quantifies the total discharge flow between two penetrating vessels. The relative PTCS, which is the ratio of the PTCS to the total cerebral blood flow, quantifies the haemodynamic coupling between arteriolar and venular input/output. PTCS maps are represented in Fig. 5, where the thickness of the link between two spheres is proportional to the PTCS intensity. All the above quantities were evaluated using an algorithm adapted to the specific structure of the data and coded in C language.

In order to quantify the relation between couplings and spatial location more accurately, for each pair of penetrating vessels  $i$  and  $j$ , we computed the Euclidean distance  $d_{ij}$  between vessel lumen centres. Considering the extent matrix built over the inverse distance

$$\begin{aligned} E_{ij} &= \frac{1}{d_{ij}} \text{ for } i \neq j \\ E_{ij} &= 1, \end{aligned} \quad (2)$$

we tested the correlation between the PTCS map and the inverse distance matrix  $E_{ij}$ . This correlation was tested by using the Mantel test with the ade4 R package (Dray and Dufour, 2007).

The similarity between two partitions can be evaluated by computing their mutual information (MI) (Gan and Chung, 2005). This quantity represents a distance between two distinct partitions of a vascular network. Interestingly, it depends only on the partitions themselves, not on the labels assigned to them. MI is thus particularly well suited to the comparison of partitions when the identifiers are arbitrary numbers. The MI considers either deterministic or probabilistic labelling. In the case of APT and VPT, since there is no overlap between regions, each vascular segment has a distinct and deterministic label for each given territory. In the case of overlapping territories (AT and VT), different labels are possible for segments in cross-over regions. By giving a uniform probability to each possible region, we computed the MI between preferential and non-preferential territories, which is a useful criterion for quantifying image-matching quality. More precisely, for any given pair of territories ( $T_i, T_j$ ) the MI matrix is given by

$$MI(T_i, T_j) = MI_{ij} = \sum_{T_i, T_j} p(T_i, T_j) \ln \left( \frac{p(T_i, T_j)}{p_1(T_i)p_2(T_j)} \right) \quad (3)$$

where  $p(T_i, T_j)$  is the joint probability distribution of the labels and

$$p_1(T_i) = \sum_{T_j} p(T_i, T_j), \quad p_2(T_j) = \sum_{T_i} p(T_i, T_j) \quad (4)$$

MI reaches its highest value for identical graph partitions, although the labels are different in each region. This value is not 1 in general. In this paper, we normalised the mutual information using

$$MI(T_i, T_j) / \max(MI(T_i, T_i), MI(T_j, T_j)), \quad (5)$$

so 1 represented identical partitions and 0 independent partitions.

## Statistics

Comparisons were made using Student t-tests.

## Results

### Arterial and venular territories

These territories were determined by following the blood flow entering the network from each penetrating vessel. Decreasing positive flow rates determined AT, while increasing negative ones determined VT.

### Spatial structure

It should be mentioned that all the territories together spanned a large fraction of the total network volume, 88.4% for the 37 AT and 99.2% for the 24 VT. Because of overlaps between territories, representing the cross-bridging regions was not straightforward. Hence, overlapping regions are shown in white in Fig. 2A, B whereas non-overlapping ones are coloured red for AT and blue for VT, depending on whether they represent arterial perfusion or venous drainage. White overlapping regions make up a significant portion of the total network volume (47.4% for AT and 69.9% for VT), suggesting a fair amount of robustness in the micro-vascular network. The robustness index (ARI) equalled one in less than half the total vascular volume (40.9%). Regions with VRI of one represented 29.3% of the total vascular volume. These data therefore show that 60% of the vascular network is supplied by several arteries and 70% is drained by several venules.

### Robustness map (RM) distribution

To assess the network robustness more quantitatively, Fig. 2C and D, respectively, show the arterial and venous RM through the whole cortical depth. The colour of the vascular segments shows the local robustness index (RI), ranging from 1 in red to 32 in blue, associated with arterial perfusion (Fig. 2C). Conversely, RI goes from 1 in blue to 22 in red for the venous drainage (Fig. 2D).

These maps illustrate how penetrating vessels are inter-connected through their ramifications at each level of the cortex from the surface to deeper regions. The overlap between territories can rise to 32 different arteriolar entries (the blue collecting veins indicated in Fig. 1C). The same qualitative observation can be made for Fig. 2D, where red (arteriolar) segments are shown to discharge their flux into up to 22 different veins.

This important topological observation differs significantly from the usual anatomical idea of veins collecting blood from one or a few neighbouring arteries. The reality of coupling is thus more complex than expected, which is why more detailed analyses are needed to establish a systematic coupling map between penetrating vessel inputs/outputs. We calculated the histogram of distribution of the RI among vessels. This provided a very accurate quantitative evaluation of possible collateral perfusion between territories. An RI equal to one corresponds to the absence of collateral flows whereas a larger RI indicates more arteriole supplies. The arterial RI histogram (Fig. 3a) shows a large range of values as RI can go up to 32. It indicates that 63% of the segments have RIs between 1 and 5. Then, it drops quickly: 22% of the vascular segments have RIs between 6 and 10 and 9% of them have RIs between 11 and 16. A very large number of lateral supplies is rare (5% of the segments have an RI between 16 and 20, and less than 2% an RI greater than 20). This observation is further supported by the semi-logarithmic representation (Fig. 3A), where the linear histogram variation suggests an exponential probability distribution of RI among vessels. Fitting the linear trend indicates the slope, the inverse of which provides an estimation of the average. Average ARI was found to be ten, indicating that, on average, each vessel can be supplied by ten different arteries. Similar qualitative

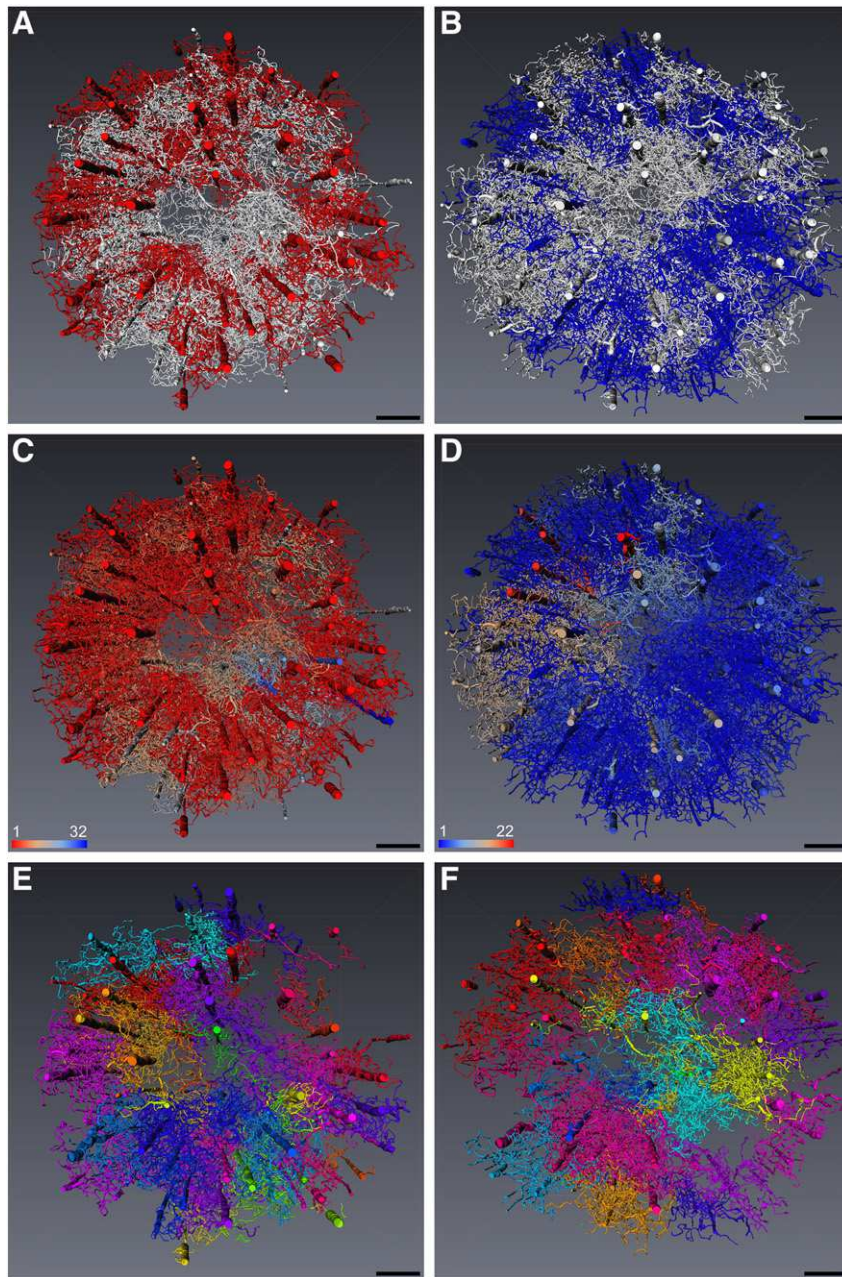


**Fig. 2.** Vascular territories and robustness maps: arteriolar territories (AT in red, A) and venular territories (VT in blue, B) are characterised by overlapping regions which are displayed in white (A, B). Arteriolar (C) and venular (D) robustness maps are computed using the robustness index (RI) values for each vascular segment (colour coding: from 1 (red) to blue (32) in (C), from 1 (blue) to 22 (red) in D). Arteriolar preferential territories (APT, E) and venular preferential territories (VPT, F) are illustrated using different colours. Scale bar = 500  $\mu\text{m}$ .

information was obtained for the venous side (Fig. 3B), for which we found a similar average VRI of 14.

Finally, we also evaluated the RI variations within the whole cortical depth, as shown in Fig. 3C and D. By averaging the RI of all vessel segments inside serial 250-micrometer-thick sections of the cortex parallel to the brain surface, it was found that the average arteriolar RI increased from 1 to 7 through the cortical depth, with a large increasing step in the middle part of the cortex. It reached its highest value in the deeper layers of the cortex (Fig. 3C). In cases of venular RI, the average RI was also increased in the lower half of the cortical depth, where it kept a fairly constant level, with a maximum average value of 4 (Fig. 3D). These results show a global increase of robustness with cortical depth.

### Preferential territories

By construction, the preferential territories (PT) illustrated in Fig. 2E and F represent non-overlapping regions associated with draining venules (VPT) and penetrating arterioles (APT) respectively. As opposed to perfusion drainage territories AT and VT that occupy nearly the whole vascular volume, the sum of PT volumes covers 58.8% of the total network volume for APT and 40.5% for VPT. Hence, compensation from haemodynamic coupling which may occur in the dual complementary regions of APT can use 41.2% of the micro-vascular volume. This is consistent with the previous estimation of an overlapping AT volume fraction of 47.4%.

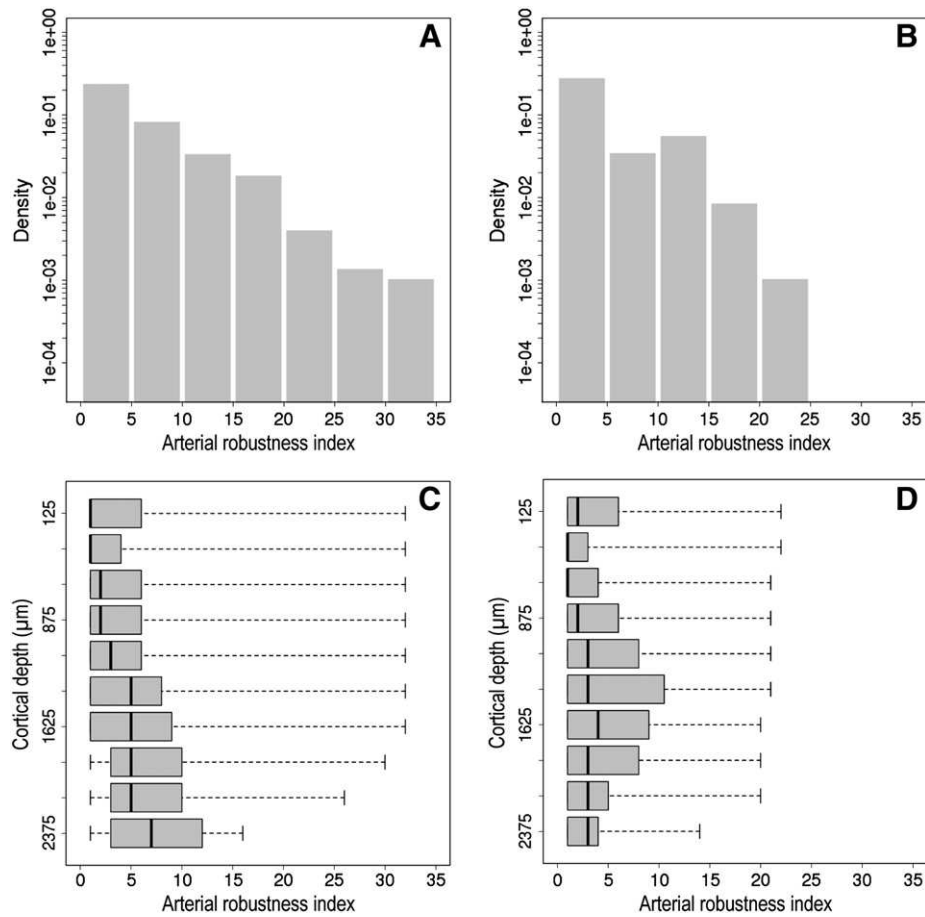


**Fig. 3.** Robustness distribution inside the vascular network. The distribution of robustness index RI among vessels (in semi-logarithmic representation, A and B) shows the possible collateral perfusion between arterial (A) or venous (B) territories. The distribution of RI (box plot representation, C and D), averaged inside 250- $\mu\text{m}$ -thick sections, varies as a function of the cortical depth in arterial (C) and venous (D) territories (on the ordinate axis, top corresponds to the upper, and bottom to the lower part of the grey matter).

We note that APT and VPT seem to share similar spatial extents. They may not all extend from the top to the bottom of the cortex. Some invade a limited portion of the cortical depth (for example supplementary figure E, the blue and green APT on the left). Quantitative analyses presented in Fig. 4 show that VPTs do not significantly differ from APTs in terms of vascular volume (respective means 0.028 and 0.027  $\text{mm}^3$ ,  $p=0.8$ ) and vessel length (respective means 55.6 mm and 38.3 mm,  $p=0.2$ ).

As expected, preferential territories were 7 to 8 times shorter than AT and VT, which is the consequence of their respective definitions, since the spatial extent of a given PT is restrained by the presence of its neighbours. Nevertheless, the APT volumes did not differ significantly from the AT ones, a result which may be attributed to the considerable contribution of large arteriolar trunks, which are present in both APT and AT, to the territory volume. Risser et al. (2009) showed that they represented almost half the total vascular volume. A more detailed comparison between VT and AT showed that VTs were significantly larger (0.071 and 0.044  $\text{mm}^3$  on average respectively,  $p=0.059$ ) and longer (432.5 mm and 257.3 mm on average respectively,  $p=0.055$ ) than ATs. This observation could be attributed to the smaller number of venous outputs compared to the number of arteriolar inputs (approximately 1/3 and 2/3 of penetrating vessels respectively).

#### Overlap and coupling between territories

Based on the observation of intricate patterns between inputs and outputs, we performed a systematic investigation of the overlap and

coupling maps associated with penetrating vessels. We first considered the overlap between any pair of ATs (Fig. 5A, B) and any pair of VTs (Fig. 5C, D), considering either volume (Fig. 5A, C) or flow (Fig. 5B, D).

Local patterns of overlapping volumes were observed for AT (Fig. 5A right lower part) and for VT (Fig. 5C left upper part), and more homogeneously distributed patterns of overlapping flows with, however, consistent coupling patterns for volumes and flows. The Mantel test for the distance/coupling correlation provided a significant result in the case of overlapping AT and VT volumes ( $p=10^{-4}$ ) and flows ( $p=10^{-4}$ ), so the input and output couplings are preferentially located between neighbours, in terms of structure and haemodynamics.

When the intricacy of arteriolar inputs with venular outputs is considered in terms of overlapping volumes (Fig. 5E and F) the whole graph appears to show little regional clustering. The Mantel test for distance/coupling correlation confirms this qualitative view ( $p=0.71$ ). Nevertheless, this is not true for arteriolar/venular flow overlapping, which is found to be statistically regionalised ( $p=0.01$  for distance/flow Mantel test correlation) although preferential flows for the nearest vessels are not clearly identifiable in Fig. 5F.

Hence, from the haemodynamic point of view, territories are preferentially coupled with their neighbours whatever their type (arteriolar/arteriolar, venular/venular or arteriolar/venular). In contrast, from an anatomical point of view, we found that, although volume overlapping preferentially occurred between neighbouring AT or neighbouring VT, this was not the case for arteriolar/venular territories. This can be explained by the complex entanglement of many

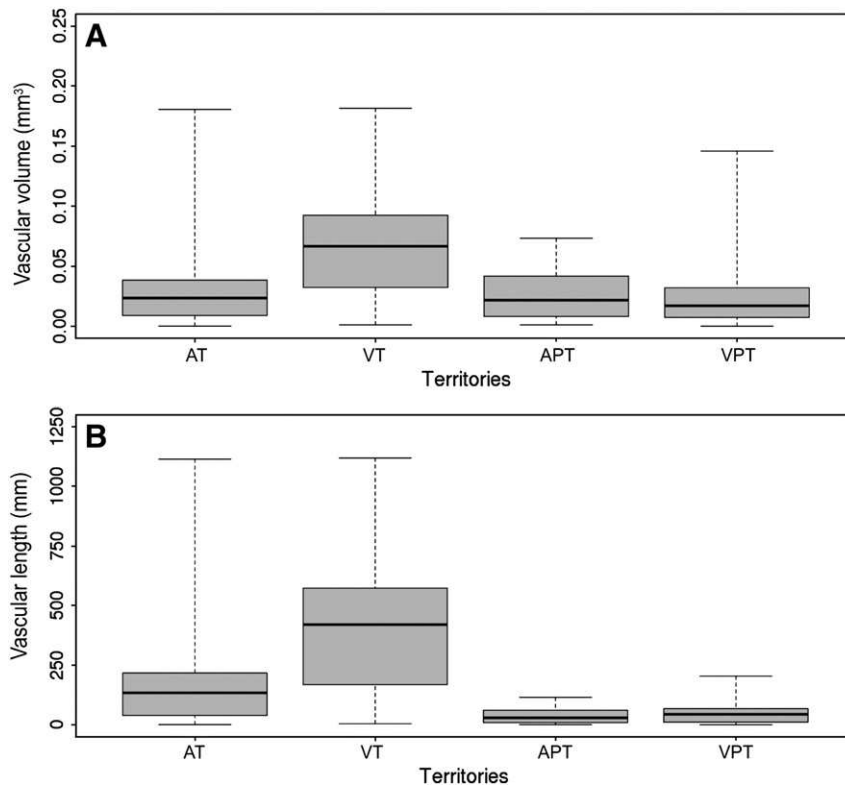


**Fig. 4.** Size distribution of the vascular territories: statistical characteristics (box-plot) of vascular volume (A) and vascular length (B) of the arterial (AT) and venous (VT) territories and of the preferential, arterial (APT) and venous (VPT), territories.

different territories through the capillary network although their pial origin may be far away.

A more functionally relevant haemodynamic quantity associated with the specific discharge of arteriolar territories into venular ones is represented by the preferential territories cross-stream (PTCS). PTCS were computed for each arteriolar input in order to measure how much flow was split up into venular outputs. The coupling map for the PTCS displays very specific local preferential flow of a given artery into collateral veins at the pial surface, illustrated by the thick lines between red spheres and nearby blue spheres in Fig. 5H. Intensities of the couplings are not always preserved between structural and haemodynamic maps, since the overlapping volumes between APT and VPT of Fig. 5G correlate moderately with the flux coupling of Fig. 5H. Anatomical overlapping thus quantitatively differs from haemo-dynamic coupling, but qualitatively provides the location of possible and preferential coupling between arterial inputs and venous outputs.

The Mantel correlation test with the distance matrix of the PTCS map also supports the presence of local couplings ( $p = 10^{-4}$ ). This observation is confirmed quantitatively: 61.5% of the flow of each arteriole is drained into its very first preferential vein whilst 83.6% goes into the first two preferential veins, as detailed in the histogram of Fig. 6.

Finally, we compared preferential and non-preferential territories using the normalised mutual information (MI), which is an indicator of similarity between partitions. We found the MI close to one-half for both arterial, AT and APT, (0.48) and venular, VT and VPT, (0.46) comparisons. This indicates that, although these territories have similar volumes, they are not particularly similar as far as vessel topology is concerned. They nevertheless share almost half of their vascular segments, which is consistent with previous observations that 40.9% of the segments of vascular territories are fallible regions. However,

we found a very small MI of 0.148 between AT and VT, which is consistent with a small, but non-zero overlapping between these regions.

## Discussion

We found that a penetrating arteriole perfused a vascular volume of  $0.03 \text{ mm}^3$  on average and that this volume was similar in preferential and robust territories. This suggests that this vascular volume can be considered as an essential provider of blood to the cortex, since the associated cortical tissue volume depends strongly on these vessels for its perfusion. Considering that the relative vascular density of the cortex considered was 3.19% (Risser et al., 2009), the tissue volume equivalent to the  $0.03 \text{ mm}^3$  vascular territory was  $0.94 \text{ mm}^3$ . It could be assimilated to a cylinder with a calculated radius of  $386 \mu\text{m}$  around the penetrating arteriole through the cortical depth (currently  $2 \text{ mm}$ ). Interestingly, analyses of flow changes induced by local clots in penetrating arterioles in rodents found that the preservation of average flow emerged  $300\text{--}350 \mu\text{m}$  away from the affected vessel and that tissue hypoxia was centred around the clotted vessel (Nishimura et al., 2006, 2007; Zhang and Murphy, 2007), over a distance similar to the size of focal lesions attributed to ischemia in the human brain (Suter et al., 2002; White et al., 2002).

Thus experimental and simulation data converge towards results suggesting that the penetrating arteries should be considered as a bottleneck (Nishimura et al., 2007). The prevalence of such regional organisation is also supported by the fact that perfusion/drainage territories preferentially overlap their volumes and flows with neighbours. There is, moreover, strong perfusion coupling between arterioles and venules, since more than 60% of a particular arterial flow is drained by a nearby venule. The micro-vascular network may thus be considered as a juxtaposition of vascular units associating one arteriole and one or two preferential neighbouring venules.

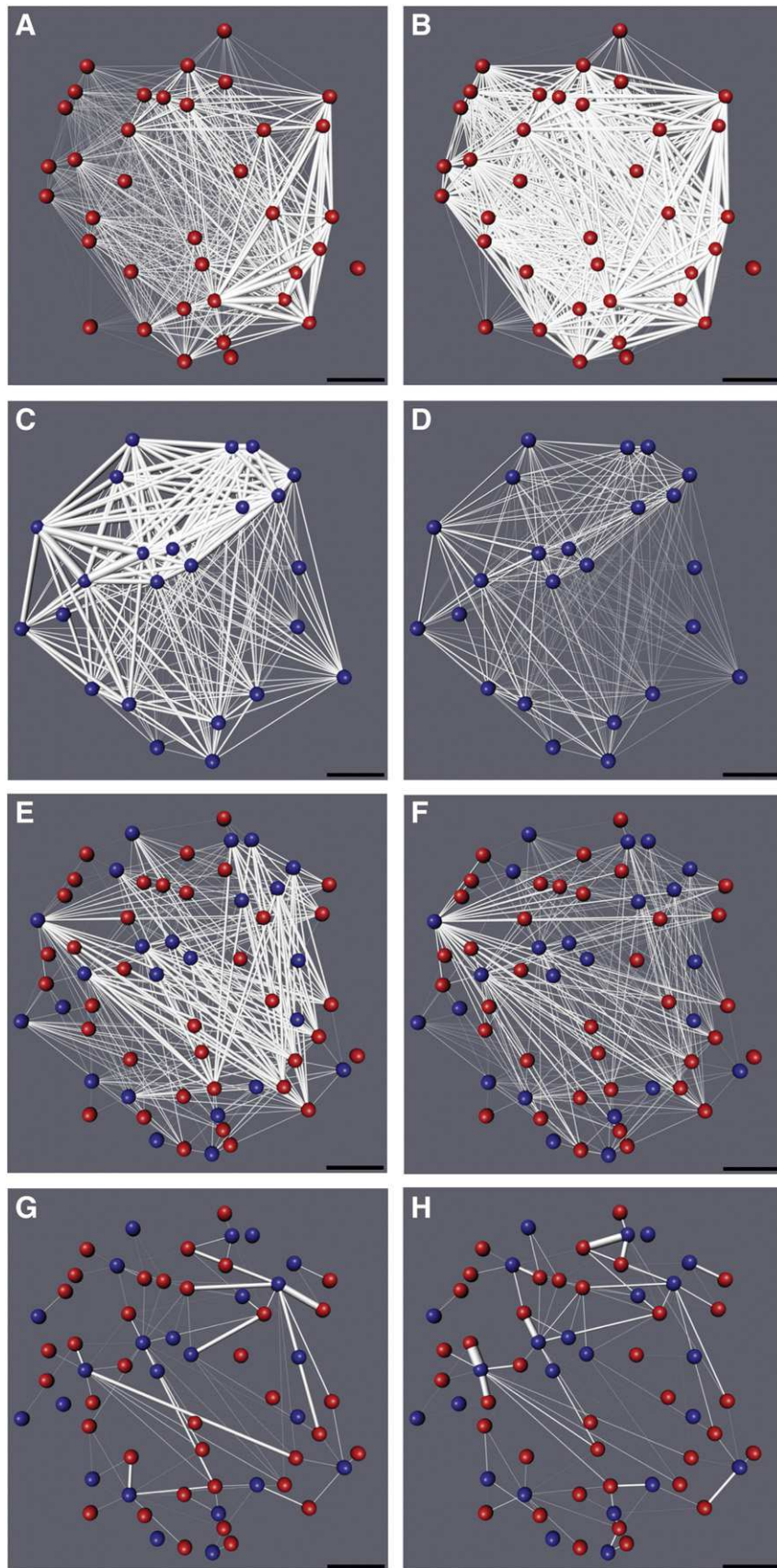


**Fig. 5.** Couplings between arterial and venular territories. Spatial (A, C, E, G) and flow (B, D, F, H) couplings between territories (A–F) or preferential territories (G–H). Overlaps and couplings are represented in a 2D plane from the pial inputs (in red)/outputs (in blue) by white lines. The thickness of the links is proportional to the overlap intensity (measured by the normalised shared volumes or flows between pairs of territories AT and VT, A–F), or of the coupling (measured by the relative cross-stream between preferential territories APT and VPT, G–H). Scale bar: 500  $\mu\text{m}$ .

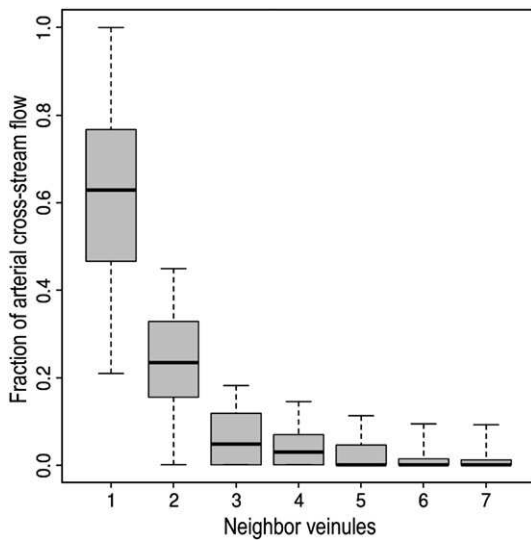


**Fig. 6.** Preferential arterial venous/drainage. More than 60% of each arteriole flow is drained by a single venule, and more than 20% by a second one.

Nevertheless, although very localised preferential functional couplings between penetrating arterioles and venules exist in terms of blood flow, their locations do not follow any identified spatial pattern, as illustrated in Fig. 5. Systematic nearest neighbour coupling patterns such as those qualitatively described by Duvernoy et al. (1981) or arteriolar hexagonal patterns proposed by Bar (1980) may be oversimplified anatomical views.

Besides such local vascular domains centred around penetrating arterioles, our results also support an alternative, more diffuse, organisation with capillary-mediated supply. The simulation of blood flow inside a large realistic vascular network “at rest” associating structural (morphological and topological) as well as functional (blood flow) data, suggests that the vascular network is organised so that considerable passive blood redistribution is possible within the vasculature. Several quantitative elements have been identified, which presently support this viewpoint.

Thus, although robust and preferential territories have similar volumes, their lengths are significantly different. This difference is explained by the contribution of small-diameter vessels, which contain minute volumes of blood. Consequently, the topology of the vascular network differs between the two types of territories. The arterial territory spreads over longer distances from the penetrating vessel than the preferential ones (APT), with the assumption that vessel distribution is homogeneous at this scale (Risser et al., 2007). Furthermore, we found that the volume overlap between arteriolar and venular territories did not present a statistically significant regionalised structure, so a diffuse distributed overlap between the cortex input/output mediated by the capillary network also exists.

Moreover, the restriction of the vascular organisation into independent distinct units would miss nearly 50% of the cortical vascular volume: we showed that territories overlap by more than 47% of their volume and that complementary regions of preferential territories occupy 41%.

We have also found that segments receiving blood from only one artery represent 40.9% of the total vascular volume and 28.2% of the total number of vascular segments. These segments roughly correspond to the population of segments with a diameter greater than 11.2  $\mu\text{m}$ , which constitutes 48% of the vascular volume (Risser et al., 2009). Therefore, they are not capillaries. On average, a segment, and probably a capillary segment, can be potentially fed by ten different arterioles. This suggests that compensation for arterial input can reach high values for a substantial population of vascular segments.

Finally, the convergence between arteriolar input and venular output can be very high, as one vein can collect blood from 32 arterioles, with an average value of 14 arterioles. This is different from the theoretical value of 2 found for the case of strict nearest neighbour vascular units (due to the ratio of arteries/venules).

Hence, although we found very local functional couplings between preferential arterio/venular partners, we also brought out large potential collateral supplies, which can extend over a surprisingly large spatial volume. Hence, we found that passive collateral supply is important and, although penetrating arterioles are the bottleneck of brain perfusion, approximately half the vascular volume can receive blood from neighbouring penetrating vessels. These results are relevant to the normal physiological function of the primate brain. The question of how the territories and their coupling could change in a dynamic or pathological context will need to be considered in future studies.

Moreover, our approach pinpoints local variations in the robustness index through the cortical depth. It increases regularly from the top to the bottom of the cortex, with a significant increase in the second half of the cortex thickness. This suggests that, the deeper a vascular segment is situated, the larger is the number of feeding arteries and so the possible compensation. In consequence, the drastic effects on blood speed observed in several generations of branches downstream of a clot-obstructed penetrating arteriole, when an experimental approach was used (Nishimura et al., 2007), may not apply to the whole vessel network, since the experimental exploration is technically limited to the upper part of the cortex. Interestingly, infarct volumes generated by occlusion of intra-cortical arterioles do not present a regular cylindrical shape around the damaged arteriole, but a rather conical shape having its base in the upper cortical layers (Blinder et al., 2010). This observation suggests that compensation is positively correlated with cortical depth, which we have shown to be associated with an increasing index of robustness. Therefore collateral supply would be larger in lower cortical layers than in the upper ones.

## Conclusions

Our results paint a new picture (sketched on Fig. 7) of the intra-cortical perfusion in the primate brain, highlighting a large capacity of the vascular network for compensatory flow.

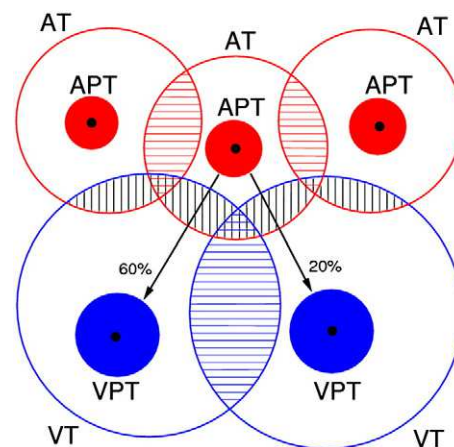


**Fig. 7.** Synthetic schematic representation of the most salient characteristics of vascular territories investigated in this paper. Their size, volume overlap, and perfusion coupling are analysed and quantified. They show both local preferential functional perfusion coupling between preferential arteriolar (APT) and venular (VPT) territories (thus 80% of one arteriolar blood is drained by two close venules) and large, distributed possible supply (high mean arteriolar (ARI=10) and venular (VRI=14) robustness index). Dashed red or blue lines indicate overlap between arteriolar (AT) or venular (VT) territories, which represent respectively 2/3 and 1/3 of penetrating vessels symbolised with black discs.

The results obtained by our numerical approach are in agreement with experimental data obtained by other studies showing the local specific perfusion of cortical tissue by penetrating arterioles. Almost half of the vascular volume is potentially sensitive to blood supply deficiency from the pial matter. It is mainly located in the upper part of the cortical depth, where arteriolar vessels are more numerous. Our study also points out the large potential supply in the other half of the vascular volume, where an average of ten overlapping territories per vascular segment can be found. This robust volume is mainly composed of capillaries and is mostly found in the lower half of the cerebral cortex. This finding is particularly interesting considering the relevance of capillaries in blood flow control and pathophysiological processes (Itoh and Suzuki, 2012).

In addition, our numerical approach discriminates between the spatial and functional coupling of territories. Neighbouring arterioles or venules are significantly coupled, sharing more vascular segments and blood flow with close arterioles or venules than with distant ones. This configuration would support a capacity for local compensation in blood supply or draining. In addition, arteriolar and venular territories simultaneously have long-distance anatomical couplings and preferential local haemodynamic convergence. Hence the functional contribution of the vascular network to the passive perfusion would be relevant for local compensatory protection, even though the capillary network can link distant territories. The large possibilities of supply that we have revealed inside the primate cortex might represent a second level of robustness for correctly supplying the cortical parenchyma. The first one is provided by the organisation of the pial network into anastomosed arteries (Duvernoy et al., 1981; Schaffer et al., 2006) and interconnected arterial loops (Blinder et al., 2010), which limit damage to the cortical tissue in case of obstruction. In this context we may wonder whether there is a superposition between the loops of the pial arterial network and the preferential spatial coupling between intracortical arterioles.

## Funding

This work was supported by a PhD grant from Paul Sabatier Toulouse 3 University to RG, funding (AO3) from the Scientific Board of Paul Sabatier Toulouse 3 University, and by the Centre National de la Recherche Scientifique (project PEPH “Analyse morphométrique des réseaux vasculaires et neuronaux”).

## Acknowledgments

We thank Pr. A. Steyer for fruitful discussions.

### Disclosure statement

The authors disclose no conflict of interest.

## References

- Bar, T., 1980. The vascular system of the cerebral cortex. *Adv. Anat. Embryol. Cell Biol.* 59, 1–62 (I–VI).
- Bell, M.A., Ball, M.J., 1985. Laminar variation in the microvascular architecture of normal human visual cortex (area 17). *Brain Res.* 335, 139–143.
- Blinder, P., Shih, A.Y., Rafie, C., Kleinfeld, D., 2010. Topological basis for the robust distribution of blood to rodent neocortex. *Proc. Natl. Acad. Sci. U. S. A.* 107, 12670–12675.
- Cassot, F., Lauwers, F., Lorthois, S., Puwanarajah, P., Duvernoy, H., 2009. Scaling laws for branching vessels of human cerebral cortex. *Microcirculation* 16, 331–344 (332 pp. following 344).
- Dray, S., Dufour, A.B., 2007. The ade4 package: implementing the duality diagram for ecologists. *J. Stat. Softw.* 22, 1–20.
- Duvernoy, H.M., Delon, S., Vannson, J.L., 1981. Cortical blood vessels of the human brain. *Brain Res. Bull.* 7, 519–579.
- Fonta, C., Imbert, M., 2002. Vascularization in the primate visual cortex during development. *Cereb. Cortex* 12, 199–211.
- Fung, Y.C., 1997. *Biomechanics, Circulation.* Springer-Verlag.
- Gan, R., Chung, A.C., 2005. Multi-dimensional mutual information based robust image registration using maximum distance-gradient-magnitude. *Inf. Process. Med. Imaging* 19, 210–221.
- Guibert, R., Fonta, C., Plouraboue, F., 2010a. Cerebral blood flow modeling in primate cortex. *J. Cereb. Blood Flow Metab.* 30, 1860–1873.
- Guibert, R., Fonta, C., Plouraboue, F., 2010b. A new approach to model confined suspensions flows in complex networks: application to blood flow. *Transp. Porous Media* 83, 171–194.
- Hamel, E., 2006. Perivascular nerves and the regulation of cerebrovascular tone. *J. Appl. Physiol.* 100, 1059–1064.
- Harel, N., Bolan, P.J., Turner, R., Ugrubil, K., Yacoub, E., 2010. Recent advances in high-resolution MR application and its implications for neurovascular coupling research. *Front. Neuroenergetics* 2, 130.
- Itoh, Y., Suzuki, N., 2012. Control of brain capillary blood flow. *J. Cereb. Blood Flow Metab.* <http://dx.doi.org/10.1038/jcbfm.2012.5>. [Electronic publication ahead of print].
- Kiani, M.F., Hudetz, A.G., 1991. A semi-empirical model of apparent blood viscosity as a function of vessel diameter and discharge hematocrit. *Biorheology* 28, 65–73.
- Liebesskind, D.S., 2003. Collateral circulation. *Stroke* 34, 2279–2284.
- Nishimura, N., Schaffer, C.B., Friedman, B., Tsai, P.S., Lyden, P.D., Kleinfeld, D., 2006. Targeted insult to subsurface cortical blood vessels using ultrashort laser pulses: three models of stroke. *Nat. Methods* 3, 99–108.
- Nishimura, N., Schaffer, C.B., Friedman, B., Lyden, P.D., Kleinfeld, D., 2007. Penetrating arterioles are a bottleneck in the perfusion of neocortex. *Proc. Natl. Acad. Sci. U. S. A.* 104, 365–370.
- Nishimura, N., Rosidi, N.L., Iadecola, C., Schaffer, C.B., 2010. Limitations of collateral flow after occlusion of a single cortical penetrating arteriole. *J. Cereb. Blood Flow Metab.* 30, 1914–1927.
- Plouraboué, F., Cloetens, P., Fonta, C., Steyer, A., Lauwers, F., Marc-Vergnes, J.P., 2004. X-ray high-resolution vascular network imaging. *J. Microsc.* 215, 139–148.
- Pries, A.R., Secomb, T.W., 2005. Microvascular blood viscosity in vivo and the endothelial surface layer. *Am. J. Physiol. Heart Circ. Physiol.* 289, H2657–H2664.
- Risser, L., Plouraboue, F., Steyer, A., Cloetens, P., Le Duc, G., Fonta, C., 2007. From homogeneous to fractal normal and tumorous microvascular networks in the brain. *J. Cereb. Blood Flow Metab.* 27, 293–303.
- Risser, L., Plouraboue, F., Descombes, X., 2008. Gap filling of 3-D microvascular networks by tensor voting. *IEEE Trans. Med. Imaging* 27, 674–687.
- Risser, L., Plouraboue, F., Cloetens, P., Fonta, C., 2009. A 3D-investigation shows that angiogenesis in primate cerebral cortex mainly occurs at capillary level. *Int. J. Dev. Neurosci.* 27, 185–196.
- Rossier, J., 2009. Wiring and plumbing in the brain. *Front. Hum. Neurosci.* 3, 2.
- Schaffer, C.B., Friedman, B., Nishimura, N., Schroeder, L.F., Tsai, P.S., Ebner, F.F., Lyden, P.D., Kleinfeld, D., 2006. Two-photon imaging of cortical surface microvessels reveals a robust redistribution in blood flow after vascular occlusion. *PLoS Biol.* 4, e22.
- Sigler, A., Goroshkov, A., Murphy, T.H., 2008. Hardware and methodology for targeting single brain arterioles for photothrombotic stroke on an upright microscope. *J. Neurosci. Methods* 170, 35–44.
- Suter, O.C., Sunthorn, T., Kraftsik, R., Straubel, J., Darekar, P., Khalili, K., Miklossy, J., 2002. Cerebral hypoperfusion generates cortical watershed microinfarcts in Alzheimer disease. *Stroke* 33, 1986–1992.
- Weber, B., Keller, A.L., Reichold, J., Logothetis, N.K., 2008. The microvascular system of the striate and extrastriate visual cortex of the macaque. *Cereb. Cortex* 18, 2318–2330.
- White, L., Petrovitch, H., Hardman, J., Nelson, J., Davis, D.G., Ross, G.W., Masaki, K., Launer, L., Markesbery, W.R., 2002. Cerebrovascular pathology and dementia in autopsy Honolululu-Asia Aging Study participants. *Ann. N. Y. Acad. Sci.* 977, 9–23.
- Woolsey, T.A., Rovainen, C.M., Cox, S.B., Henegar, M.H., Liang, G.E., Liu, D., Moskalkenko, Y.E., Sui, J., Wei, L., 1996. Neuronal units linked to microvascular modules in cerebral cortex: response elements for imaging the brain. *Cereb. Cortex* 6, 647–660.
- Zhang, S., Murphy, T.H., 2007. Imaging the impact of cortical microcirculation on synaptic structure and sensory-evoked hemodynamic responses in vivo. *PLoS Biol.* 5, e119.
- Zheng, D., LaMantia, A.-S., Purves, D., 1991. Specialized vascularization of the primate visual cortex. *J. Neurosci.* 11, 2622–2629.